Magnetic Field Measurements of a Twisted Flux Rope in a Failed Solar Eruption

New Jersey Institute of Technology

Yuqian Wei, Bin Chen, Sijie Yu, Haimin Wang, Ju Jing and Dale E. Gary

New Jersey Institute of Technology

Abstract

Magnetic flux ropes are the centerpiece of solar eruptions. Direct measurements for the magnetic field of flux ropes are crucial for understanding the triggering and energy release processes, yet they remain heretofore elusive. Here we report microwave imaging spectroscopy observations of an M1.4-class solar flare occurred on 2017 September 6, using data obtained by the Expanded Owens Valley Solar Array. This flare event is associated with a failed eruption of a twisted filament observed in H-alpha by the Goode Solar Telescope at the Big Bear Solar Observatory. The filament, initially located along the magnetic polarity inversion line prior to the event, undergoes a failed eruption during the course of the flare. This partially erupting filament has a counterpart in microwaves, whose spectral properties indicate gyrosynchrotron radiation from flare-accelerated nonthermal electrons. Using spatially resolved microwave spectral analysis, we derive the magnetic field strength along the filament spine, which ranges from 700--1400 Gauss from its apex to the legs. The results agree well with the non-linear force-free magnetic model extrapolated from the pre-flare photospheric magnetogram. The multi-wavelength signatures of the event are consistent with the standard scenario of eruptive flares, except that the eruption failed to fully develop and escape as a coronal mass ejection. We conclude that the failed eruption is likely due to the strong strapping coronal magnetic field above the filament.

Introduction

Main scientific goal:

Provide measurement of the spatially resolved magnetic field along an active filament in a flare-productive Active Region

Microwave Diagnostics: Gyrosynchrotron

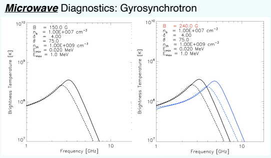

Fleishman et al. 2020

Temporal Res.	1s
Freq Range	1-18GHz
Elements	13
Longest Baseline	1.5 km

EOVSA

An example of Gyrosynchrotron emission in Magnetic Flux Rope(MFR)

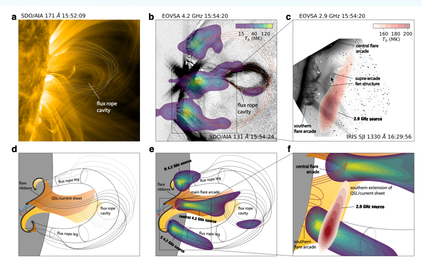

Chen et al. 2020a

Observation

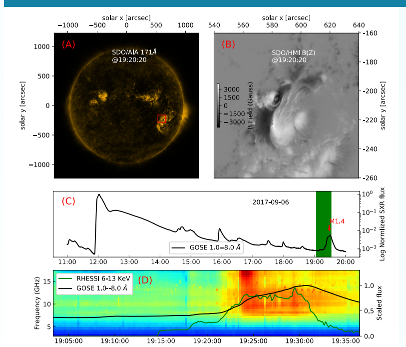

M1.4 Flare
Sep.6th 2017
Peaked:
19:24:00 UT

Data Coverage:
EOVSA
BBSO/GST
RHESSI

Fig1: (A) AR 12673 as observed in EUV by the SDO/AIA 171˚A filter band on 2017 September 6 at 19:20:20 UT. (B)Detailed view of the SDO/HMI radial photospheric magnetogram of the core region of the AR (red box in (A)). (C) GOES 1–8A soft X-ray (SXR) light curve from 11 UT to 20 UT on 2017 September 6. The M1.4 flare event under study (marked by the red arrow and the green shaded region) occurs during the late decay phase of the large X9.3 flare (SOL2017-09-10T12:24:00).(D) Background subtracted EOVSA microwave dynamic spectrum from 19:03 UT to 19:37 UT. The black and green curves are for RHESSI 6–13 KeV X-ray and GOES 1–8A light curves, respectively.

Observation

A **pre-existing filament** is seen by BBSO/GST in Hα line center images before the onset of the event at 19:07:50 UT

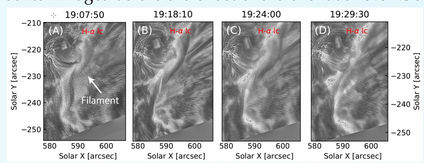

Fig2:(A)—(D) BBSO/GST Halpha line center image at four selected times during the event. The filament is marked by the white arrows in the first frame.

Microwave counterpart of the filament is observed by EOVSA. The microwave source at both frequencies show an elongated shape stretched along the north-west and south-east direction, parallels to the brightened filament seen in the SDO/AIA 304Å images.

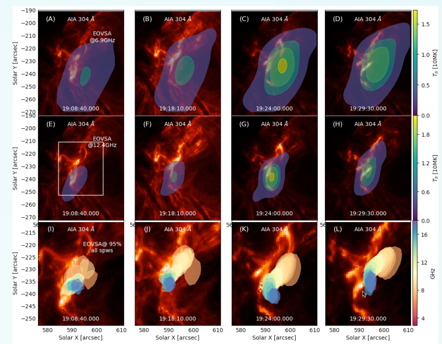

Fig3:Spatial evolution of EOVSA microwave spectroscopic images. (A -- D) Contours of the EOVSA image at 6.9 GHz is over-plotted on SDO/AIA 304A images at selected for times, as same as those in the previous figure. (E -- H) Same as (A -- D), but for the EVOSA 12.4 GHz image. (I -- L) 95% of the maximum brightness at each frequency contours of EOVSA SPW 7 -- 30 (6.4 -- 17.9 GHz) images on SDO/AIA 304A images with a smaller FOV shown as the white rectangle in (E).

Observed filament is reproduced in ***NLFFF*** extrapolated magnetic field. Reconnection Geometry (below the MFR) is revealed by the ***HXR*** and ***EUV*** observations

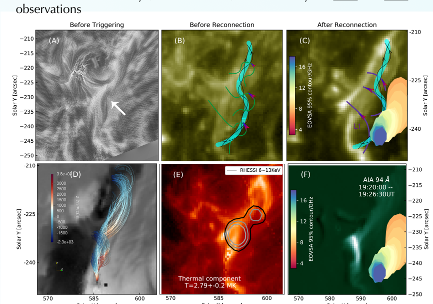

Observation

Fig4: (A) The filament as seen by BBSO/GST in Hαline center image before the onset of the event at 19:07:20 UT(denoted by the white arrow). (B) and (C) Schematic of the reconnection induced by the rising filament. The green field linesin (B) and purple field lines in (C) are pre-reconnection and post-reconnection field lines, respectively. The background is thecorresponding SDO/AIA 1600A image showing the two bright ribbons during the post-reconnection phase. EOVSA 6.4–15.9GHz images at 19:26:30 are also shown in (C) as color contours (90% of the maximum). (D) Selected field lines near the PILregion derived from the NLFFF results based on the SDO/HMI vector magnetogram at 19:00 UT. (E) RHESSI 6–13 keV X-raysource (65%, 85%, and 95% of the maximum) overlaid on SDO/AIA 304A EUV image during the impulsive phase. (F) Basedifference SDO/AIA 94A image (19:26:30 - 19:20:00 UT) showing the bright post-reconnection flare arcade. EOVSA 6.4–15.9GHz images (pre-flare-background subtracted in the image domain) at 19:26:30 are also shown.

The synchronized motion of: ***Microwave source kernel*** and ***Dark Filament front*** indicate that the source comes from the upper part of the flux rope.

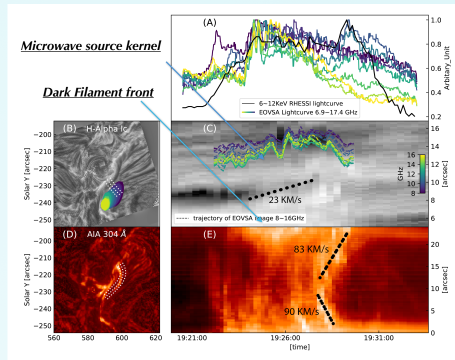

Fig5: (A) The solid black line indicates the RHSSI X-ray lightcurve at 6 – 13 keV. The EOVSA lightcurves in 7.9 – 17.4 GHz are color-coded by frequencies, as shown in the color bar in (C). (B) 90% contour of EOVSA SPW 10 – 25 (7.9 – 15.9 GHz) image contour and the cut slit (white slit) plotted on BBSO/GST Hαimage at 19:20:20 UT. (C)Time-distance stack plot of BBSO/GST Hαimage from 19:20:00 UT – 19:33:00 UT. The color-coded dashed lines indicate the location of EOVSA images. The dark filament front is pointed by two white arrows. (D) cut slit (white slit) along the filament is plotted on SDO/AIA 304A image at 19:20:20 UT. (E) The time-distance plot along the filament in SDO/AIA 304A image, showing the filament heating and material draining.

Results

12 points are selected along the microwave counterpart of the MFR (8 out of 12 are plotted). The corresponding background subtracted spectrum is fitted to the isotropic gyrosynchrotron to obtain the ***magnetic field strength*** (and other 3 free parameters, number density of thermal and non-thermal electrons, energy index of non-thermal electrons) at each point.

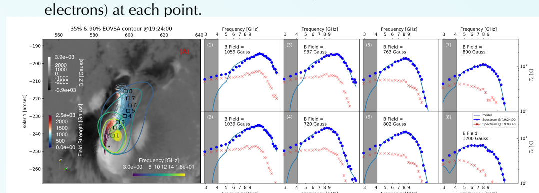

Fig6: The brightness temperature spectra in 8 points along the flux rope. (A) LOS viewing of the flux rope structure in the NLFFF extrapolated and EOVSA image (pre-flare-background subtracted in the image domain) at selected frequencies in6.9 – 17.9 GHz with 35% and 90% contour level over plotted on a photospheric magnetic field map in the Z component. Points1 – 8 correspond to spectras in (1 – 8). (1 – 8) temporal evolution of the brightness temperature spectra at point 1 – 8 in (A).The spectra at 19:24:00 UT and the best fit model(solid blue circles with error bar and solid blue line). The pre-flare spectra at each points are plotted as the red crosses in (1 – 8).

Results

Microwave diagnostics reveals a reasonable distribution of the four parameters along microwave counterpart of the MFR. The accelerated electrons are concentrated at the southern foot point. The ***magnetic field strength decreases*** with increasing distance from the footpoints.

A field line in the ***NLFFF*** extrapolated magnetic field, which goes through the 12 points, is selected to be compared with the microwave diagnostics. The results are qualitatively ***consistent***.

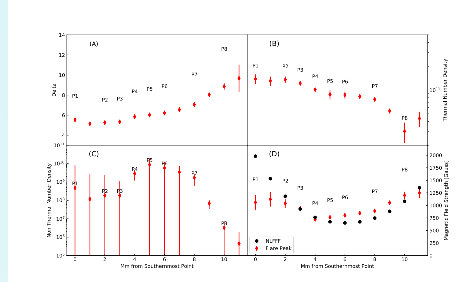

Critical free parameters' distribution along with a selected magnetic field line in the extrapolated vector coronal magnetic field. The error is constrained by Markov chain Monte Carlo (MCMC) sampling methods.
(A -- D) Spatial distribution of power-law index, thermal electron density, non-thermal electron density, and magnetic field strength, respectively. 8 plotted points in Fig6 have been anontated with number. (D) the magnetic field strength of the extrapolated field line are plotted as black dots.

The cool, dense filament is chromospheric-temperature material supported near the concave-upward ***bottoms*** of the MFR field lines. Meanwhile, accelerated electrons due to magnetic reconnection induced by the failed eruption of the MFR can enter the extended MFR cavity following the newly reconnected field lines, producing the multi-frequency nonthermal microwave emission ***above*** the filament.

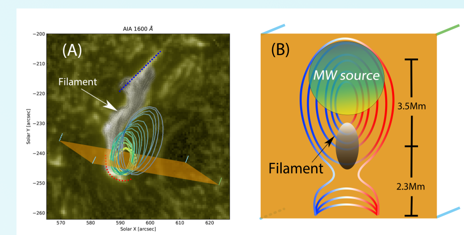

Schematic cartoon that shows the relation between the filament and the microwave source. (A) 80% contours of EOVSA images SPW (6.9 -- 15.9 GHz) image contour are plotted over the filament from Halpha image. (B) Schematic cartoon of the cross-section of the flux rope, is made out of the orange surface in (A).

Conclusion

We provide the first measurement of the spatially resolved magnetic field along an active filament in a flare-productive AR. The microwave-constrained results are qualitatively consistent with those derived from the NLFFF extrapolation.